A Novel Approach of High Resolution Imaging using Modified Excitation Signal for Ground Penetration Radar (GPR) Applications

Homayoun Ebrahimian [1], Mohammad Ojaroudi [2], and Sajjad Ojaroudi [3]

[1] Department of Electrical Engineering
Ardabil Branch, Islamic Azad University, Ardabil, Iran
ebrahimian@iauardabil.ac.ir

[2] Department of Electric and Electronic Engineering
Ankara University, Ankara, Turkey
ojaroudi@ankara.edu.tr

[3] Young Researchers and Elite Club
Germi Branch, Islamic Azad University, Germi, Iran
s.ojaroudi.p@gmail.com

Abstract ─ In this paper a modified Gaussian pulse stimulus is employed to improve the accuracy of underground pipe localizing for 2D visualization of GPR results. This pulse shaping puts more energy at higher frequencies in contrast with conventional Gaussian in GPR. Hence, a wider bandwidth is available to achieve higher accuracy for precise spatial localization. Two dimensional simulations of GPR profiles over ground surface with and without conduits run with the finite-difference time-domain (FDTD) program GPRMAX are presented to validate the accuracy of the proposed method. Results from these surveys showed decent structural recovery of a small pipe similar in structure to that of the modeled ones. Finally, the dense surveys served as a benchmark to compare interpretations taken with the same surveys at lower spatial resolutions and profiles with 2D-only processing methods in order to understand errors in analysis and interpretation that are possible from 2D surveys.

Index Terms ─ Finite Difference Time Domain (FDTD), Gaussian Pulse, Ground Penetrating Radar (GPR), Pulse Shape Modulation (PSM).

I. INTRODUCTION

Ground penetrating radar is a type of nondestructive testing (NDT) techniques which uses electromagnetic waves to investigate the composition of non-conducting materials either when searching for buried objects or when measuring their internal structure. Information that can be obtained from GPR includes the depth, orientation, size and shape of buried objects, and the density and water content of soils [1]. The GPR performance is associated with the electrical and magnetic properties of local soil and buried targets. The choice of the central frequency and the bandwidth of the GPR are the key factors in the GPR system design. Although the higher frequencies are needed for better resolution and detailed echo to determine small size objects, the lower frequencies are preferred to detect something buried too deep because of the dramatically increased attenuation of the soil with increasing frequency. Thus, the pulsed GPR is used in order to benefit from both low and high frequencies. The pulsed GPR systems acquire pulse response in time domain directly.

A challenging problem in GPR is resolution improvement. Typically, if a GPR system has insufficient resolution, small or closely-spaced targets may be smoothed together into a single aberration in the waveform. This effect may not only obscure some targets, but it also may lead to inaccurate reflection readings. Rise time, settling time and pulse aberrations of the stimulus signal can also significantly affect a GPR system's resolution [2]-[3]. Also, many factors contribute to the accuracy of a GPR results. These factors include the GPR system's impulse response, probe and interconnect reflections and material losses, impulse amplitude accuracy, baseline correction and the accuracy of the reference reflection used in the measurements.

In this paper, we explore the advantages of generating a novel stimulus, similar to the traditional signal but instead of an impulse like (Gaussian) signals, a modified signal using new codes will be employed. The advantage conferred by "high resolution GPR" is that more energy is available at higher frequencies than with conventional step or impulse GPR, subsequently a relatively higher bandwidth and higher accuracy in

Submitted On: December 31, 2014
Accepted On: May 1, 2016

identifying the reflected voltage is achieved [4-5]. Simulated results using GPRMAX software are presented to validate the effectiveness of the proposed method for precisely calculating the time-dependent location of underground targets. The GPRMAX2D is electromagnetic wave software for GPR modelling [6]. It is based on FDTD method. In this work, we choose this simulator because of its simplicity of use and rapidity. The modified GPR code has a wider bandwidth that leads to higher accuracy localization of the various buried targets. Therefore, the GPR results in modified case follow the reference buried target more closely than does the ordinary GPR results with Gaussian pulse.

II. THEATRICAL BACKGROUND AND IMPLEMENTATION OF GPR IMAGING

This section describes the reflected voltage of microstrip discontinuity using the proposed stimulus signals and compares it with simulated reflected voltage obtained using ideal impulse and step GPRs. In order to illustrate the proposed method performance, a step-slit microstrip discontinuity with the listed design parameters were simulated (Fig. 1 (a)), and the GPR results of the input impedance for both using full-wave analysis using full wave GPR results using GPRMAX2D simulation tools are presented and discussed [7]-[8]. The proposed GPR test field with circular cylindrical pipe located underground is shown in Fig. 1 (a). Figure 1 (b) present the scan B which represents the passing over a zone in which simulated GPR was buried in horizontally position (a) and the result obtained by simulation (b). It can be observed that in the case of real measurements, the image is very noisy, containing, in addition, clutters. Using the specific technology of ultrasound examinations, the image from Fig. 1 (b) is a B scan made from 171 raw data A-scan type using GPRMAX2D.

The GPR characteristics for the proposed ground surface with pipe with Gaussian pulse as stimuli in Fig. 1 (b), obviously ideal impulse provides excellent time localization, corresponding to an extremely broad frequency bandwidth in the frequency domain. Typically, for ideal impulse excitation we can calculate exactly the amount of reflected energy at an interface as follows:

$$\Gamma_{1,2} = \frac{\sqrt{\varepsilon_{r1}} - \sqrt{\varepsilon_{r2}}}{\sqrt{\varepsilon_{r1}} - \sqrt{\varepsilon_{r2}}}, \quad (1)$$

where Γ is the reflection coefficient and ε_{r1} and ε_{r2} are the dielectric constants. Similarly, for ideal impulse excitation signal we can calculate precisely the thickness of a layer as follows:

$$d_i = \frac{C.t_i}{\left(2\sqrt{\varepsilon_{r,i}}\right)}, \quad (2)$$

where d_i is the thickness of layer i, t_i the total travel time through that layer, C is the speed of light and $\varepsilon_{r,i}$ the dielectric constant of the layer where L is the transmission line length, and ε_r is the relative permittivity of substrate. The penetration depth of GPR waves (in a low-loss medium) can be approximated as:

$$\delta(m) = 25\lambda = 25\frac{c}{f\sqrt{\varepsilon_r}}. \quad (3)$$

The vertical resolution (in a low-loss medium) is given roughly as:

$$R = \delta/100. \quad (4)$$

Ideal impulse provides excellent time localization, corresponds to an extremely broad frequency bandwidth in the frequency domain. For ideal impulse as excitation signal we can calculate exactly locations of discontinuities as follows, but in practice one can see that the waveform is distorted after the reflection and propagation. Because GPR receives signals already reflected from some distance, the time needed for passing the way back to the object and forth is longer than in a case when the antenna is situated slightly above the examined object. Because of this the cross-section of a pipe will be presented in the reading as a hyperbole.

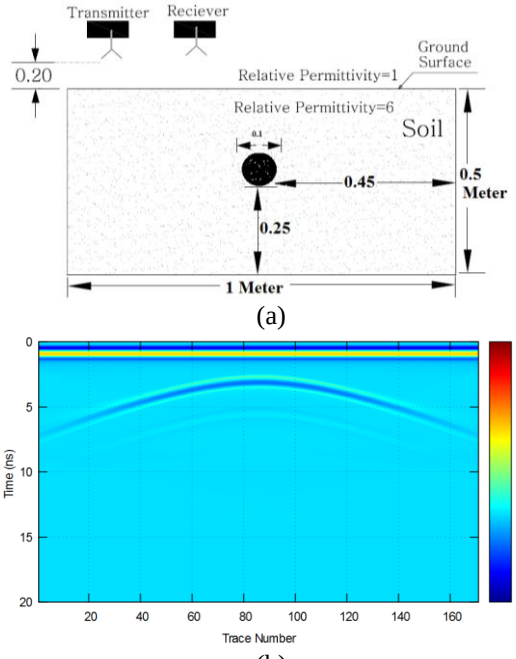

Fig. 1. Configuration of the proposed GPR test field with circular cylindrical pipe located underground, (a), scan B which represents the hyperbolic reflection from the pipe using GPRMAX 2D (b).

III. MODIFIED EXCITATION SIGNAL GENERATION BASED ON GAUSSIAN PULSE DERIVATIVES

The Gaussian pulse function $G(t,\tau)$ is part of a standard set of functions [9]. It is worth to note that

Gaussian pulses remain Gaussian distribution when they pass through any linear systems. A general formula of Gaussian pulse is shown in Equation (5), in which τ is a time constant. Gaussian monocycle is the first derivative of the Gaussian pulse and Gaussian doublet is the second derivative of a Gaussian pulse [10]. The general formulas for Gaussian monocycle and normalized Gaussian doublet are shown in Equations (6) and (7) respectively. These three signals with their spectrums are shown in Fig. 2 (a):

$$G(t,\tau) = e^{-\left(\frac{t-t_0}{\tau}\right)^2}, \tag{5}$$

$$\frac{dG(t,\tau)}{dt} = -\frac{t-t_0}{\tau} e^{-\left(\frac{t-t_0}{\tau}\right)^2}, \tag{6}$$

$$\frac{d^2G(t,\tau)}{dt^2} = \left[1-4\pi\left(\frac{t-t_0}{\tau}\right)^2\right] e^{-2\pi\left(\frac{t-t_0}{\tau}\right)^2}. \tag{7}$$

The Gaussian derivative functions have many interesting properties and will be reviewed here. When we take derivatives with respect to t (i.e., time derivatives) of the Gaussian function repetitively, we see a pattern emerging of a polynomial of increasing order, multiplied with the original (normalized) Gaussian function again. Examples are given for Gaussian derivative functions from order 0 up to order 2 (note the marked increase in amplitude for higher order of differentiation) are shown in Fig. 2. Figure 2 (b) shows normalized power spectra for Gaussian derivative filters, where the normalized power spectra shows it indicates that higher order of differentiation means a higher center frequency for the band-pass filter.

The Gaussian function itself is a common factor of all these higher order derivatives. We extract the polynomials by dividing the expression by the Gaussian function. These polynomials are the Hermite polynomials. They emerge from the following definition:

$$\frac{\partial^n e^{-t^2}}{\partial t^n} = (-1)^n H_n(t) e^{-t^2}. \tag{8}$$

The function $H_n(t)$ is the Hermite polynomial, where n is called the polynomial order. When we make the substitution $t \to \frac{t}{(\tau\sqrt{2})}$, we get the following relation between the Gaussian function $G(t,\tau)$ and its derivatives:

$$\frac{\partial^n G(t,\tau)}{\partial t^n} = (-1)^n \frac{1}{(\tau\sqrt{2})^n} H_n\left(\frac{t}{\tau\sqrt{2}}\right) G(t,\tau). \tag{9}$$

The amplitude of the Hermite polynomials explodes for large t, but the Gaussian envelope suppresses any polynomial function behavior. No matter how high the polynomial order is, the exponential function always dominates.

In this study, a novel method for designing a new excitation signal with high resolution characteristic for GPR is presented and illustrated in Fig. 3. A schematic of our new pulse shaping method, indicates that the system is comprised of three parts: differentiator, summation, and differentiator multiplier. The overall operation is generally given by M_N and represented by:

$$M_N(t) = \sum_{n=0}^{N} P_n . \frac{\partial^n G(t,\tau)}{\partial^n t}. \tag{10}$$

Specifically, formulas (11) and (12) show two examples of UWB pulses that can be used as stimulus waveforms in this study. Figure 4 shows these pulses with ordinary Gaussian pulse:

$$M_1(t) = p_0 . x(t) + p_1 \frac{dx(t)}{dt}, \tag{11}$$

with $p_0 = 1$ and $p_1 = 1$. M_1 provides the closest functional fit to the types of pulse shapes produced by our experimental hardware. Meanwhile, M_2 represents the third order of proposed method we called it waveform:

$$M_2(t) = p_0 . x(t) + p_1 \frac{dx(t)}{dt} + p_2 \frac{d^2x(t)}{dt^2}, \tag{12}$$

with $p_0 = 1$, $p_1 = 1$ and $p_2 = -1$.

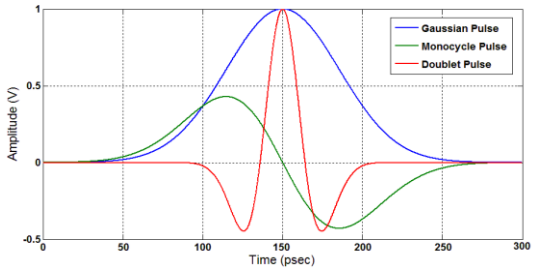

(a)

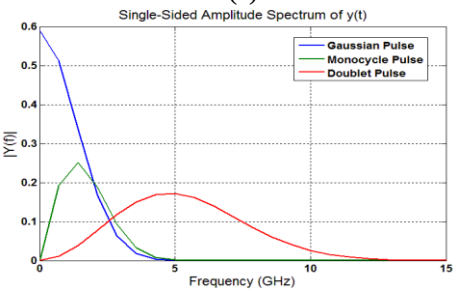

(b)

Fig. 2. Excitation waveforms used in the GPR simulations: (a) Gaussian pulse, monocycle pulse and normalized doublet pulse, and (b) frequency spectrum of each pulse. Gaussian derivative kernels act like band-pass filters [10].

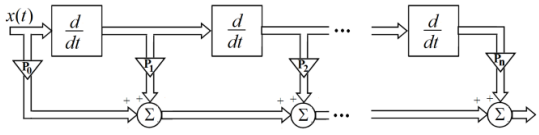

Fig. 3. The proposed schematic related to new excitation signal method.

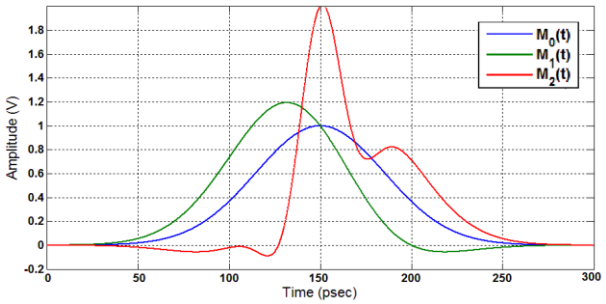

Fig. 4. The three first orders of stimulus signals generated by the proposed method used in the step GPR simulations.

IV. THE PROPOSED PULSE PERFORMANCE IN GPR RESULTS

Through processing raw data, simulated result by using GPRMAX, the image is achieved and shown in Fig. 5. Figure 5 shows the original image, before image signal processing using the excitation signals shown in Fig. 2 (a). The black and white lines are from the strong direct wave and surface reflection. Under them, three different metal objects are clearly distinguished. But the PVC pipe's image is not clear. Also, several small scatters were founded. According to the resolution, the depth resolution in the vertical plane and the distance resolution between two objects can be considered. The depth resolution of the ten of centimeters is obtained. The reason of lower depth resolution is that the lower frequency range is used. The measurements show that the developed UWB-GPR system has a good ability in detecting buried metal object, even small targets of several centimeters.

To improve the resolution of the GPR results and to show the effects of the proposed excitation signal generation method on these improvements, Fig. 5 shows the simulated reflection waveform with different shapes of our proposed excitation signal observed at the receiver. The corresponding results generated by M_1 and M_2 stimuli are shown in this figure. Two cases are studied for modified codes GPR. Using higher order coded stimulus leads better similarity to the ideal case. It is clearly shown to that GPR results with this proposed excitation signal have very good localization resolution and the peak amount errors at the center of discontinuities locations from ideal GPR results are small in this case in our simulation [11]. It is apparent from this figure, Fig. 6, that the energy in the modified GPR reflection exceeds the energy in the conventional GPR reflection. Additionally, in order to show the performance of the proposed method in multiple and complicated objects case, Fig. 7 shows another example with a pair of horizontal buried objects. As shown in Fig. 7, the modified GPR results follow the target more closely than does the ordinary step GPR results. Figures 6 and 7 indicate a discrepancy between simulated data and ideal results. This discrepancy is multi-reflection and assembly tolerances. The time characteristics for the GPR results are summarized in Table 1.

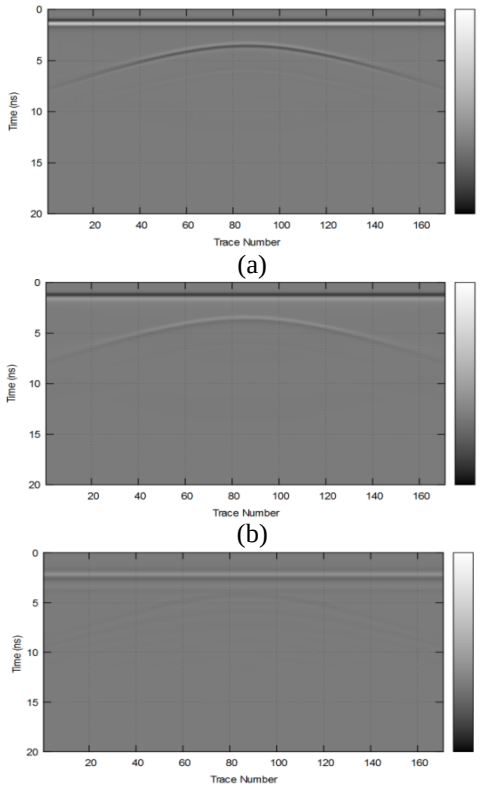

Fig. 5. GPR images before image signal processing using: (a) Gaussian, (b) monocycle, and (c) double.

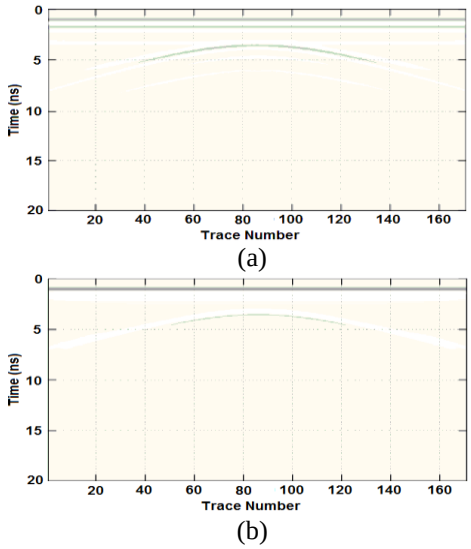

Fig. 6. GPR images after using the proposed method: (a) the first order, and (b) the second order.

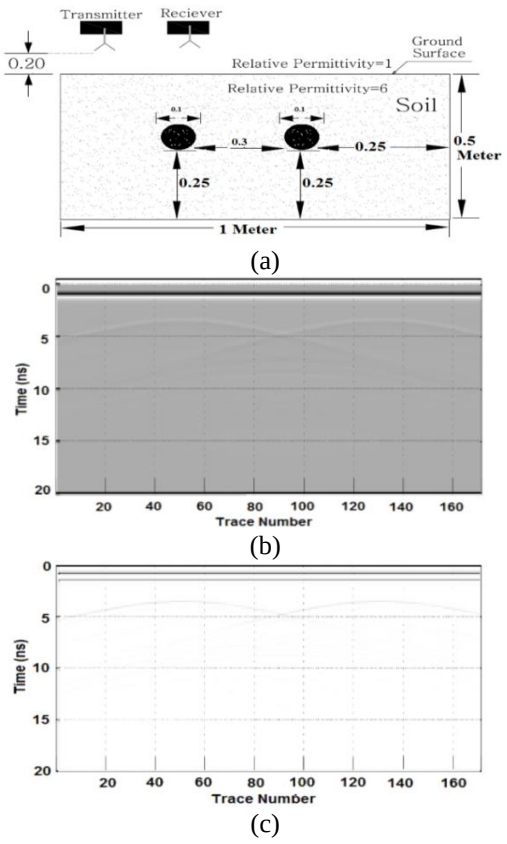

Fig. 7. (a) Configuration of the proposed GPR test field with a pair of horizontal circular cylindrical pipe located underground, (b) using conventional Gaussian pulse which represents the hyperbolic reflection from the pipes, and (c) after using the second order of the proposed method.

Table 1: The GPR characteristics of the proposed method in comparison with the ideal results

Parameter	Theoretical	M0(t)	M1(t)	M2(t)
$\Gamma_{1,2}$	-0.420	-0.39	-0.405	-0.41
d_1 (m)	0.1	0.23	0.17	0.14

V. CONCLUSION

In this paper, we present novel approach for high resolution GPR system that we designed a modified Gaussian pulse stimulus to improve the accuracy of localizing underground pipe for 2D visualization of GPR results. For the simulation the finite-difference time-domain (FDTD) program GPRMAX is used. Results obtained by our GPR system prove that our system has a good ability to finding buried targets with 1 cm resolution. The proposed modified GPR is very practical as it is based on more realistic signals rather than assuming ideal impulses. Additionally, our 2D visualization method proves that it possible to easily distinguish other buried objects. But there is one more reason why our program for 2D visualization is still in progress and improvement. Namely, we are aware that we are dealing, by the current method, with a lot of data that has to be processed in order to visualize buried objects.

REFERENCES

[1] I. Giannakis, A. Giannopoulos, and C. Warren, "A realistic FDTD numerical modeling framework of ground penetrating radar for landmine detection," in *IEEE Journal of Selected Topics in Applied Earth Observations and Remote Sensing*, vol. 9, no. 1, pp. 37-51, Jan. 2016.

[2] Z. Lin and W. Jiang, "Ground penetrating radar B-scan data modeling and clutter suppression," *2015 Fifth International Conference on Instrumentation and Measurement, Computer, Communication and Control (IMCCC)*, Qinhuangdao, pp. 397-402, 2015.

[3] S. Tan, H. Zhou, and L. Xiang, "An automatic framework using space-time processing and TR-MUSIC for subsurface imaging," *Ground Penetrating Radar (GPR), 14th International Conference on*, Shanghai, 2012, pp. 286-290, 2012.

[4] M. Ojaroudi, "Cognitive UWB imaging radar based on new approaches in cognitive visual neuroscience," *Advanced Radar Systems Journal*, vol. 3, pp. 1-7, Dec. 2014.

[5] M Ojaroudi, E. Mehrshahi, and A. Fathy, "A novel approach for the design of modified excitation signal using a narrow pulse generator for high-resolution time domain reflectometry applications," *Microwave and Optical Technology Letters*, vol. 56, no. 12, pp. 2987-2990, 2014.

[6] A. Giannopoulous, "Modelling ground penetrating radar by GprMax," *Science Direct*, pp. 755-762, 2 Aug. 2005.

[7] GPRMAX 3D/2D Software, copyright by Antonis Giannopoulos, 2005.

[8] C. Warren, A. Giannopoulos, and I. Giannakis, "An advanced GPR modelling framework: The next generation of gprmax," *Advanced Ground Penetrating Radar (IWAGPR), 8th International Workshop on*, Florence, 2015, pp. 1-4, 2015.

[9] G. E. Andrews, R. A. Askey, and R. Roy, *Special Functions*. Cambridge University Press, Cambridge, 2000.

[10] C. M. Bender and S. A. Orszag, *Advanced Mathematical Methods for Scientists and Engineers*. McGraw-Hill, New York, 1978.

[11] J. S. Lee and C. Nguyen, "Uniplanar picosecond pulse generator using step-recovery diode," in *Electronics Letters*, vol. 37, iss. 8, pp. 504-506, Apr. 2001.